Self-Assembly of Rod−Coil Diblock Copolymers

Wentao Li and Dilip Gersappe*

Department of Materials Science and Engineering, State University of New York at Stony Brook, Stony Brook, New York 11794

Received February 2, 2001; Revised Manuscript Received May 16, 2001

ABSTRACT: A two-dimensional self-consistent-field lattice model incorporating the rotational isomeric state scheme to account for chain rigidity was developed to study the phase diagram of rod−coil diblock copolymer melts. Several morphologies such as lamella, zigzag lamella, elliptical cross-sectional cylinders, and hexagonally packed cylinders were observed for rod−coil diblock copolymers. A free energy analysis suggests that the zigzag and elliptical cross-sectional cylindrical structures are metastable. The effect of decreasing the flexibility of the coil segment of a rod−coil diblock copolymer was determined. Our calculation showed that as the flexible block of the copolymer becomes more rigid, part of the cylindrical domain in the phase diagram is replaced by lamella structures.

Introduction

The self-assembly of block copolymers that contain a rigid or rodlike block has attracted a lot of interest due to their rich phase behavior and potential for use in a variety of applications. For instance, the rod fraction of rod−coil copolymers may consist of conjugated polymers, which are known to have interesting electrical and photoactive properties. Self-assembly of this type of rod−coil copolymers could produce novel electronic, optoelectronic, and optical devices. In addition, rod−coil copolymers can serve as synthetic analogues of protein-like molecules. Since protein molecules which contain both rigid and flexible sections have been shown to be the dominant component of such naturally occurring materials such as spider silk and the adhesive present in the abalone shell,[1] rigid-coil copolymers appropriately synthesized can be used to design a new class of biomimetic materials. To exploit the potential of rod−coil copolymers, however, it is necessary to be able to understand the phase behavior of these materials and to predict the types of self-assembled structures that form as a function of the architecture of the copolymer. In this paper, we adopt the rotational isomeric state (RIS) description of chain molecules and develop a two-dimensional self-consistent-field lattice model to study the phase behavior of rod−coil diblock copolymers. We identify the emergence of specific microphases in the phase diagram and also determine the conditions for the stability or metastability of these structures.

While the microphase separation of flexible diblock copolymers has been extensively studied,[2] theoretical studies of these systems typically assume that the polymer chains obey Gaussian statistics,[3−6] an assumption which is not appropriate for rigid polymer chains, such as rod−coil diblock copolymers. A theoretical analysis that accounted for chain rigidity was first performed by Semenov and Vasilenko.[7] Assuming that the rods were aligned strictly perpendicular to the lamellae, they predicted a transition from a monolayer to a bilayer structure for a rod−coil diblock copolymer. Later, Williams and Fredrickson[8] extended the work of Semenov and Vasilenko and postulated that a "hockey puck" micelle, where the rods are packed into cylinders when the volume fraction of the coil block is high, exists in the phase diagram. Muller and Schick[9] predicted that the cylindrical morphology occupies most of the phase diagram.

In the weak segregation limit, a number of studies replacing the Gaussian chain with the wormlike chain have been performed.[10] Netz and Schick[11] introduced an anisotropic interaction between semiflexible blocks. But, with their model only a symmetric semiflexible chain was studied, and they examined the formation of a lamellar morphology. Recently, by applying an exact mean-field theory to the Semenov−Vasilenko model, Matsen and Barrett[12] found that the tilted angle of a rod in a rod−coil diblock copolymer lamellar structure is controlled by competition between the rod/coil interfacial tension and the stretching of the coil block. However, their model was also limited to the lamellar structure.

In most of these theoretical treatments, the rod block of the copolymer has been treated by assuming that steric interactions tend to align all the rigid blocks with a common director. Then one can use theories developed to study liquid crystal phase behavior to model the rigid section of the copolymer, while using the Gaussian statistics to describe the flexible block. However, this approach limits the method to study structures that are already known or postulated and also makes the exhaustive exploration of phase space for new morphologies an inefficient process. For instance, Williams and Fredrickson postulated the existence of a "tightly packed micelle" but failed to derive a free energy expression to analyze its stability.

Experimental studies have revealed discrepancies between theory and experiments as a number of morphologies have been observed that have not been predicted. Chen et al.[13,14] have synthesized high molecular weight poly(hexyl isocyanate) (PHIC)−polystyrene (PS) diblock copolymers with the rod (PHIC) volume fractions ranging from 40% to over 90%. They observed "wavy" and "zigzag" patterns in the lamellar morphology for their rod−coil diblock copolymers. Radzilowski et al.[15] have synthesized rod−coil diblock copolymers with a high coil fraction, and observed structural transitions from lamellae, to a mixture of cylinder and "stripes" and then to hexagonal-packed micelle aggregates by increas-

* To whom all correspondence should be addressed.

10.1021/ma010194i CCC: $20.00
Published on Web 08/11/2001

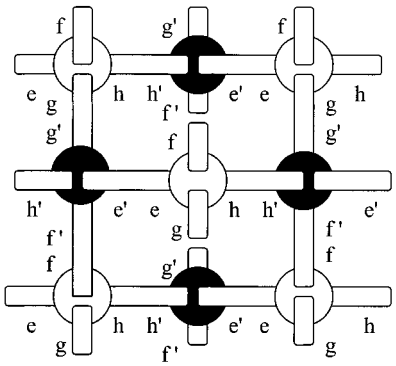

Figure 1. Segment orientation representation in a tetrahedral lattice. The same notations are adopted here as in ref 18.

ing the coil volume fraction from 64% to 75%. Stupp et al.[16] observed the supramolecular organization of a coil−coil−rod triblock copolymers into mushroom-shaped structures. In another study by Jenekhe et al.,[17] poly(phenylquinoline)−polystyrene rod−coil diblock copolymers were observed to self-organize into robust, micrometer-scale aggregates in solution.

To explain these differences and to map out the phase diagram of rigid-coil diblock copolymers, we have incorporated the RIS model to properly account for the chain rigidity in the framework of the self-consistent-field (SCF) method. Although our model is for rod−coil diblocks, we can easily extend it to study more complicated architectures. The main feature of this model is that no a priori assumption has to be made about the orientation of the rod in the morphology. Rather, the system is allowed to self-assemble into its desired structure. Further, this model will work in both the weak and the strong segregation limits, and we can incorporate asymmetry in both composition and in the rigidity of the blocks of the copolymer. Below, we present details on the model that we use in this paper and then present the results that we obtain for the phase diagram of the rod−coil diblock copolymer.

Model Description

Conformations of three successive C−C bonds in the rotational isomeric state description can be represented by three energetically most favorable states: one trans (t) and two gauche (g+, g−). The rigidity of these three C−C bonds is determined by the energy difference between the trans and the gauche state, U_g. We consider a polymer chain consisting of r segments with each segment having two bonds. Segment r_i of a polymer chain i is connected with r_{i-1} by the first bond of r_i and the second bond of r_{i-1}. The rigidity of the polymer chain is defined by a single parameter U_g. In the following we use the same notations for bond orientations as described in one-dimensional model formulated by Leermakers et al.[18] and extend the analysis to study structure formation in two dimensions.

We consider a tetrahedral (diamond) lattice as shown in Figure 1. Each site has four bond orientations denoted by e″, f″, g″, and h″. For each bond orientation two opposite directions can be distinguished, denoted as e and e′, f and f′, g and g′, and h and h′. e″, f″, g″, and h″ are orientated such that f″ and g″ connect segments in the same layer and e″ and h″ connect segments in neighboring layers. Following this construction a chain molecule can be fitted to a tetrahedral lattice with each segment occupying one lattice site.

In our model, in a system containing polymers that consist of A and B monomers, a segment of type A at site (x,y) experiences a mean-field potential, $\mu_A(x,y)$, which is given by

$$\mu_A(x,y) = \mu'(x,y) + kT\sum_B \chi_{AB}(\langle\varphi_B(x,y)\rangle - \varphi_B{}^b) \quad (1)$$

Here the first term is a "hard core" potential, which ensures the incompressibility of the system, and the second term is due to the energetic contribution from the nearest-neighbor interactions. χ_{AB} is the Flory−Huggins interaction energy between A and B monomers. $\varphi_B{}^b$ is the bulk volume fraction for segment type B, and $\langle\varphi_B(x,y)\rangle$ is called the contact fraction of A segment with B segment at site (x,y) and is expressed as

$$\langle\varphi_B(x,y)\rangle = \lambda_1[\varphi_B(x-1,y) + \varphi_B(x+1,y) + \varphi_B(x,y-1) + \varphi_B(x,y+1)] \quad (2)$$

Here λ_1 is a lattice constant and equals $^1/_4$ in a tetrahedral lattice. If we assume that the potential of a free segment is independent of the orientation of that segment, then the free segment weighting factor for segment s of type A with orientation $\alpha\beta$ (where α and β can be any of the allowed bond orientations) at site (x,y) is given by

$$G_A(x,y,s^{\alpha\beta}) = \begin{cases} 0 & \text{if } \alpha = \beta \\ G_A(x,y,s), & \text{otherwise} \end{cases} \quad (3)$$

Here the free segment weighting factor $G_A(x,y,s)$ is related to the potential experienced by the segment s of type A at site (x,y)

$$G_A(x,y) = \exp(-\mu_A(x,y)/kT) \quad (4)$$

The end segment distribution function $G_i(x,y,s|1)$ of polymer chain i, introduced in the SCF model, gives the statistical weight of all possible walks starting from segment 1, which may be located anywhere in the lattice, and ending at segment s at site (x,y). Accounting for the bond orientations the recursive relation for the end distribution function for segment s (of polymer chain i) at site (x,y) with orientation $\alpha\beta$ is then

$$G_i(x,y,s^{\alpha\beta}|1) = G_i(x,y,s^{\alpha\beta})\sum_{\gamma'}\lambda^{\beta''-\alpha''-\gamma''}G_i(x',y',(s-1)^{\gamma'\alpha'}|1) \quad (5)$$

In this case segment s at site (x,y) with the first bond in direction α is connected with segment $s-1$ at site (x',y') with the second bond in direction α'. (x',y') takes values of $(x-1,y)$, $(x+1,y)$, $(x,y-1)$, and $(x,y+1)$. $\lambda^{\alpha''-\beta''-\gamma''} = \lambda^t$ if the connection of the segment s to $s-1$ forms a trans conformation such that $\alpha'' = \gamma''$ and $\lambda^{\alpha''-\beta''-\gamma''} = \lambda^g$ if the connection of the segment s to $s-1$ forms a gauche conformation such that $\alpha'' \neq \gamma''$. The gauche and trans probabilities can be obtained from U_g with $\lambda^g = 1/[2 + \exp(U_g/kT)]$ and $\lambda^t = 1 - 2\lambda^g$. The recurrence relation of eq 5 can be started with $G_i(x,y,1^{\alpha\beta}|1) = G_A(x,y)$ if the first segment of chain i is of segment type A. Similarly, the recursive relationship

starting from the other end of the chain of length r is given by

$$G_i(x,y,s^{\alpha\beta}|r) = G_i(x,y,s^{\alpha\beta})\sum_{\gamma'}\lambda^{\beta''-\alpha''-\gamma''}G_i(x',y',(s+1)^{\gamma'\alpha'}|r) \quad (6)$$

The volume fraction of segment s at site (x,y) of polymer chain i is then

$$\varphi_i(x,y,s) = \sum_{\alpha}\sum_{\beta}C_i\,\lambda^{\alpha\beta}G_i(x,y,s^{\alpha\beta}|1)\,G_i(x,y,s^{\alpha\beta}|r)/G_i(x,y,s^{\alpha\beta}) \quad (7)$$

where C_i is a normalization constant for chain i, related to bulk volume fraction, φ_i^{b}, by the equation

$$C_i = \varphi_i^{\,b}/r_i \quad (8)$$

In the summation of eq 7 the volume fraction of a segment s in all orientations is weighted according to an a priori probability = 1/24 for each orientation.[18] A matrix formulation is given in the Appendix detailing the calculations. The free energy per chain of the system is of particular interest here as it determines the stability of the morphology of the diblock copolymer melt. The free energy per chain is given by

$$(A - A^*)/kT = \left[\sum_i\frac{\theta_i}{r_i}\ln r_iC_i - \sum_{x,y}\sum_A\varphi_A(x,y)\frac{u_A(x,y)}{kT} + \frac{1}{2}\sum_{x,y}\sum_A\sum_B\phi_A(x,y)\chi_{AB}\langle\varphi_{\mathrm{B}}(x,y)\rangle - \frac{1}{2}\sum_i(\theta_i\sum_{A,B}\varphi_{Ai}{}^*\chi_{AB}\varphi_{Bi}{}^*)\right]/\sum_{\mathrm{i}}\frac{\theta_i}{\boldsymbol{r}_i} \quad (9)$$

In this equation A^* is the free energy of the reference state, chosen as the pure amorphous state. θ_i, the total number of segments of molecule type i in the system, is given as

$$\theta_i = \sum_{x,y}\varphi(\boldsymbol{x},\boldsymbol{y}) \quad (10)$$

and $\varphi_{Ai}{}^*$ is the volume fraction of segment A in pure amorphous i, given by

$$\varphi_{Ai}{}^* = r_{Ai}/r_i \quad (11)$$

where r_{Ai} is the number of A segments of molecule type i.

The derivation of the free energy equation eq 9 can be found in ref 19.

To prevent bias of the resulting morphology, we follow the procedure of Drolet and Fredrickson,[20] and our calculation is initiated with different random potentials $u_{\mathrm{A}}(x,y)$. Then the segmental weighting factor $G_{\mathrm{A}}(x,y)$ and monomer volume fraction $\varphi(x,y)$ can be calculated. From the volume fraction, the potential, $u_{\mathrm{A}}(x,y)$, is recalculated and compared with the guess. If the two are not in close agreement, $u_{\mathrm{A}}(x,y)$ is reestimated with Newton's method, and thus an iterative loop is set up. The calculation stops when the guessed value of $u_{\mathrm{A}}(x,y)$ is within a tolerance (typically 1×10^{-6}) of the calculated value. The free energy change at this point has a difference $<1 \times 10^{-6}$ between iterations. Periodic boundary conditions are used in our calculation to minimize edge effects. The morphology obtained corresponds to either a stable or a metastable state. By comparing the free energy of the system, the relative stability of the morphologies can be assessed. We also vary our system size to make sure that the morphology emerged is not constrained by the system size and that the free energy for that structure is the lowest. Typically our system size ranges from 20×20 to 50×50 lattice sites. Our block copolymer has a structure of AB with $N_{\mathrm{A}} + N_{\mathrm{B}} = 20$. The Flory−Huggins parameter between A segment and B segment is varied from the onset of phase separation to 1, which corresponds to χN ranging from 7 to 20. χN was incremented in steps of 1 to construct the phase diagram; however, near the transition points the step length was reduced to 0.5 to improve the accuracy of the phase diagram.

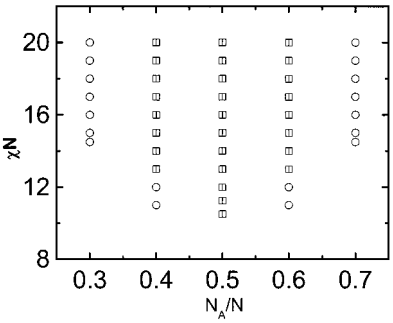

Figure 2. Phase diagram for a coil−coil AB diblock copolymer. The calculation was done with an AB diblock copolymer by varying the A faction from 30% to 70%. We fixed $N_{\mathrm{A}} + N_{\mathrm{B}} = 20$. Both the A and B segments have $U_{\mathrm{g}} = 0$. The circle represents the cylindrical structure, and the square with a line through the center represents the lamellar structure.

Lattice artifacts could arise in a lattice-based model when the interfacial thickness of a two-phase system is comparable to the size of a lattice unit. The interfacial width of the diblock copolymers we studied is more than several lattice units. The lamellar spacing and interfacial width calculated in our model are similar to the analytical results of Semenov.[21] This suggests that we did not hit the lattice limit in our calculations. In addition, our boundary condition could induce some artifacts. However, we used different initial potentials and also varied the system size to make sure that the morphology is not influenced by the particular boundary condition.

Results and Discussion

Coil−Coil Diblock Copolymer. In the first set of our results, we constructed the phase diagram of a coil−coil diblock copolymer melt as a test of our model. In this case, U_{g} for both the A and B segments is zero. We varied the fraction of A segment from 30% to 70% and obtained the phase diagram as shown in Figure 2. The critical point occurs at around $\chi N = 10.5$, which is close to theoretical prediction.[22] Our phase diagram is very similar to the one obtained by Matsen and Schick[6] except that the gyroid and cubic phases are excluded in our two-dimensional calculations. The lamellar phase is observed for a symmetric AB diblock copolymer. For 40% fraction of A or 40% fraction B, there is a transition from hexagonal-packed cylinder to lamellar structure. For 30% fraction of A or 30% fraction of B only the hexagonal-packed cylinder can be observed with χN below 20. The features in our phase diagram show

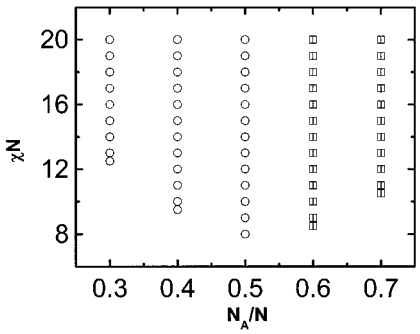

Figure 3. Phase diagram for a rod−coil diblock copolymer. In this study A is the rod block with $U_g(A) = \infty$, and B is the coil block with $U_g(B) = 0$. The circle represents the cylindrical structure, and the square with a line through the center represents the lamellar structure.

quantitative agreement with Matsen and Schick's phase diagram.

Rod−Coil Diblock Copolymer. In this study U_g for the A segment is infinite, which corresponds to $\lambda^t = 1$ and $\lambda^g = 0$, while U_g for the B segment is 0. So the A block is a rod and the B block is a coil. The phase diagram for the rod−coil block copolymer is shown in Figure 3. Note that the phase diagram is highly asymmetric. The lamellar phase occurs only at higher volume fractions of the rodlike component, while at higher coil content the only structures observed are cylindrical structures. The inverse cylinder morphology cannot occur at a high rod volume fraction for rod−coil copolymers, and this breaks the symmetry observed when both blocks are flexible. Further, the presence of the rod component changes the critical point from around $\chi N = 10.5$ for coil−coil diblock to around $\chi N = 8$ for the rod−coil diblock copolymer. These results differ from those reported by Muller and Schick, where they found that the critical point was located closer to $\chi N = 9$ and the lamellar morphology occupied a much smaller portion of the phase diagram.[9]

From the figure we can also see that the transition from the disordered to the lamella phase at higher rod contents occurs at a lower χ when compared with the transition from a disordered to a cylindrical morphology at a lower rod content. The transition between the cylindrical and the lamella morphology also occurs at a much larger rod content than observed in the flexible diblock case. Below we present details on the two primary structures observed in the calculation.

Cylindrical Morphology. We found that the cylindrical structure of the low rod fraction block copolymer (i.e., 30% rod and 40% rod) is very robust. We always obtain the cylindrical structure for these two compositions. Williams and Fredrickson[8] predicted the existence of nonlamellar structures such as monolayer puck, bilayer puck, spherically packed micelle, radially packed cylindrical micelle, and tightly packed micelle, when the coil volume fraction is high and the interaction between the rod and coil segment is low. However, as our current formulation does not allow us to obtain the rod section orientation, a direct comparison of our cylinder with their cylindrical micelle or tightly packed micelle is not easy. Nevertheless, our results suggest that nonlamellar structures, such as cylinder, may contribute significantly in the rod−coil phase diagram. In addition to cylinders, the hexagonal-packed elliptical cross-section cylinder was observed for the symmetric rod−coil diblock copolymer in all the interaction parameter range studied, from $\chi N = 7$ to $\chi N = 20$. But this structure has a higher free energy than a more rounded, hexagonal-packed cylinder. The two typical structures we found in our modeling are shown in Figure 4. Our free energy calculation indicates that the structure "E" (elliptical cylinder) has a slightly higher free energy of $-0.634kT$ per chain than the structure "C" (more rounded cross section), which is $-0.663kT$ per chain. The former has a enthalpy $H_E = -1.958kT$ per chain and entropy $S_E = -1.324k$ per chain. The latter has a $H_C = -2.036kT$ per chain and $S_C = -1.373k$ per chain. As a noncircular cross section cylinder will have a higher surface area than a circular cross section cylinder, the "E" structure pays a larger surface energy penalty, and consequently, the more circular structure is the one that is the equilibrium structure.

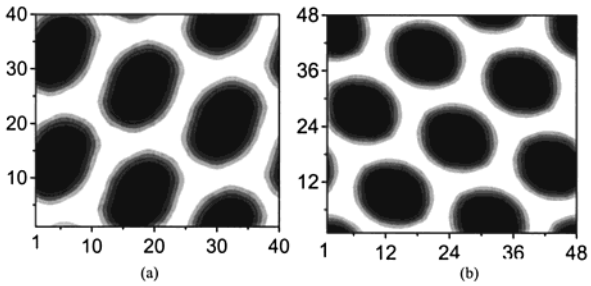

Figure 4. Examples of the observed morphology for an A10B10 rod−coil diblock copolymer. The A block is the rod block with $U_g(A) = \infty$, and the B block is the coil block with $U_g(B) = 0$. $\chi N = 15$. Regions rich in rod block A are shown in black. The structure (a) with an elliptical cross-sectional surface has higher free energy and is less stable than the more rounded structure (b).

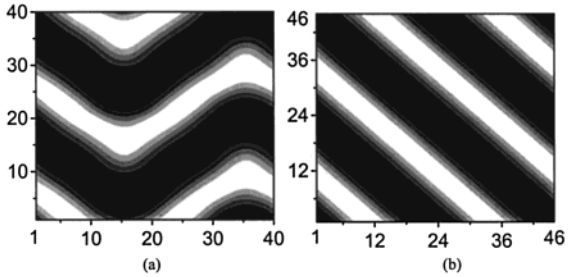

Figure 5. Examples of morphology for an A12B8 rod−coil diblock copolymer. In this case A is the rod block with $U_g(A) = \infty$, and B is the coil block with $U_g(B) = 0$. $\chi N = 13$. Regions rich in rod block A are shown in black. Please note here the different system sizes in (a) and (b).

Lamellar Morphology. When we use a rod fraction >50%, a number of interesting stable and metastable structures were observed. In this range, we have observed the stable lamellar structures, zigzag, and fragmented zigzag for 60% rod fraction diblock copolymers. When we increased the rod fraction beyond 60%, we only observed the lamellar phases.

Our modeling enables us to estimate the stability of different structures. In addition, by dividing total energy into enthalpic and entropic parts, we could identify experimental conditions for the metastable structures to occur. Figure 5 shows two typical structures we observed for rod−coil diblock copolymers with a 60% rod fraction. The regular zigzag structure was observed at the system size of 40. It is obvious from Figure 5a that this zigzag structure cannot be observed at a system size smaller than the distance between the two kinks on the zigzag structure. Only a lamellar structure has

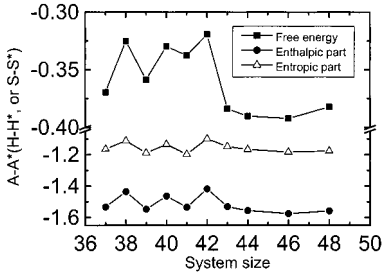

Figure 6. Free energy and its components for the rod−coil diblock copolymer system as a function of the system size. $\chi N = 13$. $A - A^*$ (the excess free energy) and $H - H^*$ (the excess enthalpy) are in the unit of kT per chain, and $S - S^*$ (the excess entropy) is in the unit of k per chain, where k is Boltzmann constant. The structures observed from system size 37 to 48 are lamella, imperfect zigzag, lamella, zigzag, lamella, distorted zigzag, lamella, lamella, lamella, and lamella, respectively. The typical structures are shown in Figures 5 and 7. Note the lowest free energy state occurs at the system size 46.

been observed in our modeling when we used small system sizes.

We note that there is a possibility either that the origin of the observed zigzag could be due to lattice artifacts or that is simply a kink that is present in the lamella structure. For example, the work of Gido et al.[23] showed the existence of a tilt grain boundary (which may manifest itself as a kinklike zigzag structure) in a coil−coil diblock copolymer melt. However, our SCF modeling of rod−coil diblocks did not show the zigzag structure in all the composition ranges and all the system sizes we studied, but only in the region that was close to what has been observed experimentally. Further, we initiated our system with different random potentials to make sure that what we see is not a result of lattice effects (such as lattice artifacts or a particular boundary condition). In addition, we note that an increase of repulsion between rod and coil segments resulted in a fragmented zigzag structure, which showed good agreement with Chen et al.'s work. We therefore believe that the zigzag structure formation is an inherent property of some rod−coil diblock copolymers. While we presently cannot identify the origin of the kinks in our zigzag structure, we believe it is likely due to a change of orientation of the rods.

To estimate the stability of the various structures, the free energy per chain is plotted as a function of the system size in Figure 6. The typical structures are given in Figures 5 and 7. Several runs were done for each system size, and the structure with lowest free energy is taken as the stable state at that system size. From the figure it can be seen that all the lamellar structures have a lower free energy. To further understand the role of enthalpy and entropy, the enthalpic and entropic contribution to total free energy is plotted in Figure 6. Note that the higher the enthalpy, the higher the free energy, while the higher the entropy, the lower the free energy, as free energy $A = H - TS$. The balance between entropy and enthalpy in these rod−coil systems can be clearly seen here. Structures that try to maximize entropy tend to have higher enthalpies, and structures that minimize enthalpic losses have lower entropies. Our free energy analysis suggests that the zigzag morphology may form when there is some condition to relieve the unfavorable interaction between rod segment and coil segment. An intuitive choice is the solvent. In the presence of a good solvent, during solvent evaporation the rod−coil block copolymer can choose the higher entropy state zigzag, as the interaction between rod and coil segment is screened. As the entropy of the system is predominately determined by the coil segment, the solvent has to be a good solvent for the coil segment or both segments. This gives good agreement with the work by Chen et al.[13,14] They found a zigzag morphology for rod−coil diblock copolymer poly(styrene-*b*-hexyl isocyanate) when toluene, a good solvent for PS (coil) block, was used as casting solvent. Their work also showed a strong dependence of their rod−coil diblock copolymer morphology on the casting solvent. This also suggests that the zigzag morphology could be metastable. When a worse solvent, like $CHCl_3$, is used as a casting solvent, the fragmented zigzag was observed. In our modeling, an increase of χ_{AB} to 0.75 and above for the 60% rod fraction block copolymer resulted in a disconnected zigzag structure as shown in Figure 8.

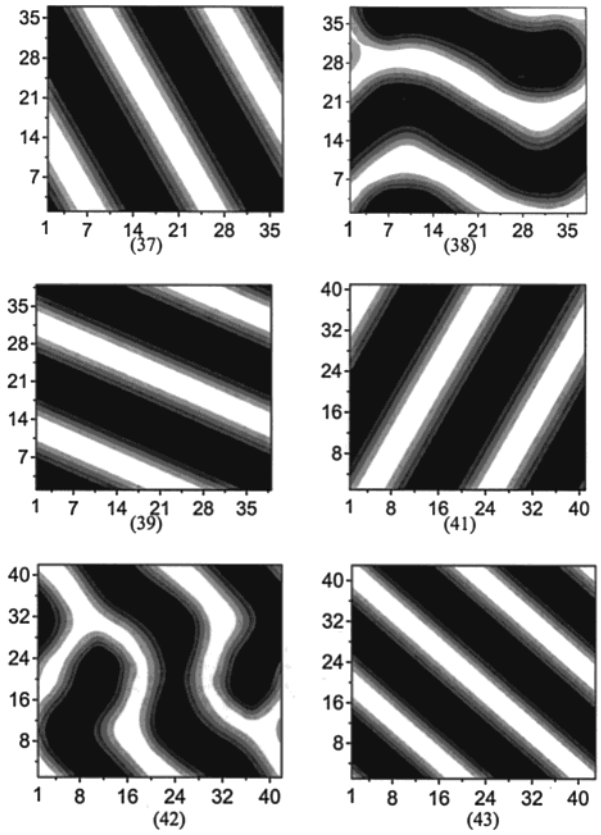

Figure 7. Structures of rod−coil diblock copolymer at different system sizes. $\chi N = 13$. The number below each graph indicates the system size. The corresponding free energy is given in Figure 6.

Rod−Semiflexible Diblock Copolymer. At a high coil volume fraction, for instance, below 40% rod fraction, only the hexagonal-packed cylindrical structure is observed for the rod−coil diblock. This structure is rather robust. Therefore, we believe that the cylindrical structure could be the only structure for rod−coil diblock copolymers with a high coil volume fraction. Our modeling also shows a transition from cylinder to lamellar when the rod faction is increased. This has been found by Radzilowski and Stupp.[15] Their rod−coil diblock copolymer showed the hexagonal packed cylinder phase at 25% rod fraction and the lamellar phase at 36% rod fraction. To compare this exact transition point, because the coil segment in practice is seldom truly flexible ($U_g = 0$ in RIS model), we proceeded to study the effect

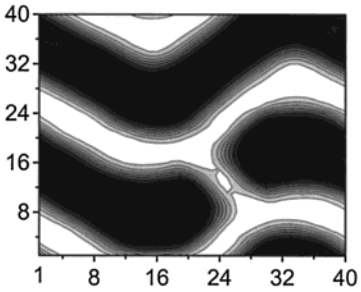

Figure 8. Examples of the disconnected zigzag structure for an A12B8 rod−coil diblock copolymer. A is the rod block, and B is the coil block. $\chi N = 18$. Please note here that the second (lower) zigzag structure is fragmented.

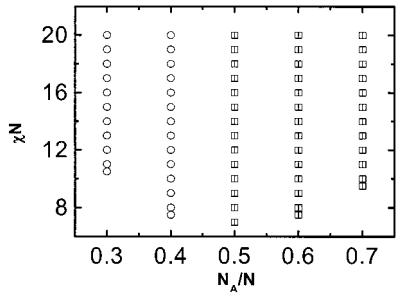

Figure 9. Phase diagram for an AB rod−semiflexible diblock copolymer. In this study the A is a rod block with $U_g(A) = \infty$, and B is a semiflexible block with $U_g(B) = 1.2$. The circle represents the cylindrical structure, and the square with a line through the center represents the lamellar structure. The cylindrical domain observed for the symmetric rod−coil diblock copolymer has been partially replaced by the lamellar structure.

of introducing some rigidity in the coil section of the diblock copolymer to determine its effect on the phase diagram.

We used a diblock copolymer AB with $U_g(A) = \infty$ and $U_g(B) = 1.2$. Its B block is slightly rigid with a persistence length of $3b$, where b is the bond length. The phase diagram is given in Figure 9. From the figure we see that, due to the entropy loss with increasing the rigidity of B block, the critical point has now decreased from $\chi N = 8$ (for a rod−coil diblock) to 7 (for a rod−semiflexible diblock). There is also a decrease of χN values for the phase separation points when compared with the rod−coil diblock copolymer. Another feature revealed in Figure 9 is that cylindrical domain for a symmetric rod−coil diblock copolymers has changed to lamellae. We expect that lamellar phase may continue to replace the cylindrical phase as the rigidity of block B is increased, and finally, only the lamellar phase will exist for rod−rod diblock copolymers. For 40% rod volume fraction the elliptical cross-sectional cylinder was also observed, but it is again less stable than the cylinder with more rounded cross section, as in rod−coil diblock copolymers. The zigzag structure was also found in the lamellar regime at a rod volume fraction of 60%.

At this stage we would like to address the transition from cylinder to lamellar phase by changing the composition of diblock copolymers. In Radzilowski and Stupp's experiment,[15] the coil segment is polyisoprene, which is rather flexible. But the whole block copolymer contains four chemically distinct segments and more looks like a tetrablock. Each segment type will have a different rigidity and interaction parameter with the rest. Its behavior could be complex, and therefore it is hard to directly compare with our modeling results. The rod−coil diblock copolymer synthesized by Chen et al.'s[13,14] is more like a truly rod−coil diblock copolymer, which contains only styrene and hexyl isocyanate segments. The lamellar morphology was observed starting from a 40% rod fraction. Polystyrene in the unperturbed state has a persistence length around $6b$,[24] a little more rigid than the B segment we investigated here. In our case, the transition lies between 40% and 50%. Thus, the matching between experiments and our model is quite good.

Summary

We have formulated a two-dimensional SCF model incorporating the rotational isomeric state scheme to study the morphology of rod−coil diblock copolymers. The phase behavior in the weak to intermediate segregation limit was investigated. Our modeling results are in good agreements with current experiments. Although our model does not include fluctuations, the RIS-based description of bond orientation can capture the realistic connectivity of segments and so should give a more realistic picture of chain behavior. In addition, the direction of rod is not predetermined, as in most existing models, and instead, the system will adjust itself to find the minimum free energy state. The orientation of rod in different structures is very interesting from both an experimental and a theoretical point of view. We are currently working on the formulation to obtain the rod orientation from the segmental weighting factors. Finally, our model can be easily extended to study rod−coil triblock or multiblock copolymers and study the solvent effect on its morphology.

Acknowledgment. We gratefully acknowledge funding from the NSF (Grant DMR 0079410). We also thank Dr. Pochan for useful discussions.

Appendix

The equations in the two-dimensional SCF-RIS model can be converted to a matrix formulation to simplify computation, similar to the one-dimensional model by Leermakers and Scheutjens.[18] In the following we first give the degeneration list for bond orientations in two-dimensional model and then give the matrix method. As shown in Figure 1, there are totally 24 orientations for a segment of two bonds. In a two-dimensional space bond orientations above and below the surface are indistinguishable. For instance, bond orientation g′f′ and fg are indistinguishable. So there are 12 numerically different orientations. In one dimension there are only seven numerically different orientations. Then we have the following degenerate segmental orientation list:

eh = h′e′, ef = h′g′, eg = h′f′, fh = g′e′, gh = f′e′, fg = g′f′

gf = f′g′, fe = g′h′, ge = f′h′, hf = e′g′, hg = e′f′, he = e′h′

The segment orientation degeneration simplifies the calculation. Now eq 5 can be written as

$$G(x,y,s|1) = G(x,y,s)\sum_{x',y'}\lambda(x',y')\,G(x',y',(s-1)|1) \quad \text{(A1)}$$

where $G(x,y,s)$ is a 12 × 12 matrix with all elements zero except the diagonal elements, which have the following values:

$$G(x,y,s)_{1,1} = G(x,y,s^{eh}),\ G(x,y,s)_{2,2} = G(x,y,s^{ef}),\ G(x,y,s)_{3,3} = G(x,y,s^{eg})$$

$$G(x,y,s)_{4,4} = G(x,y,s^{fh}),\ G(x,y,s)_{5,5} = G(x,y,s^{gh}),\ G(x,y,s)_{6,6} = G(x,y,s^{fg})$$

$$G(x,y,s)_{7,7} = G(x,y,s^{gf}),\ G(x,y,s)_{8,8} = G(x,y,s^{fe}),\ G(x,y,s)_{9,9} = G(x,y,s^{ge})$$

$$G(x,y,s)_{10,10} = G(x,y,s^{hf}),\ G(x,y,s)_{11,11} = G(x,y,s^{hg}),\ G(x,y,s)_{12,12} = G(x,y,s^{he})$$

and the four λ matrixes are all 12 × 12 with almost all elements zero. The nonzero elements are given as follows. For λ matrix $\lambda(x-1, y)$:

$$\lambda(x-1,y)_{1,1} = \lambda_t,\ \lambda(x-1,y)_{1,4} = \lambda_g,\ \lambda(x-1,y)_{1,5} = \lambda_t$$

$$\lambda(x-1,y)_{2,1} = \lambda_g,\ \lambda(x-1,y)_{2,4} = \lambda_g,\ \lambda(x-1,y)_{2,5} = \lambda_t$$

$$\lambda(x-1,y)_{3,1} = \lambda_g,\ \lambda(x-1,y)_{3,4} = \lambda_t,\ \lambda(x-1,y)_{3,5} = \lambda_g$$

For λ matrix $\lambda(x+1, y)$:

$$\lambda(x+1,y)_{10,8} = \lambda_g,\ \lambda(x+1,y)_{10,9} = \lambda_t,\ \lambda(x+1,y)_{10,12} = \lambda_g$$

$$\lambda(x+1,y)_{11,8} = \lambda_t,\ \lambda(x+1,y)_{11,9} = \lambda_g,\ \lambda(x+1,y)_{11,12} = \lambda_g$$

$$\lambda(x+1,y)_{12,8} = \lambda_g,\ \lambda(x+1,y)_{12,9} = \lambda_g,\ \lambda(x+1,y)_{12,10} = \lambda_t$$

For λ matrix $\lambda(x, y-1)$:

$$\lambda(x,y-1)_{5,2} = \lambda_t,\ \lambda(x,y-1)_{5,7} = \lambda_g,\ \lambda(x,y-1)_{5,10} = \lambda_g$$

$$\lambda(x,y-1)_{7,2} = \lambda_g,\ \lambda(x,y-1)_{7,7} = \lambda_t,\ \lambda(x,y-1)_{7,10} = \lambda_g$$

$$\lambda(x,y-1)_{9,2} = \lambda_g,\ \lambda(x,y-1)_{9,7} = \lambda_g,\ \lambda(x,y-1)_{9,10} = \lambda_t$$

For λ matrix $\lambda(x, y+1)$:

$$\lambda(x,y+1)_{4,3} = \lambda_t,\ \lambda(x,y+1)_{4,6} = \lambda_g,\ \lambda(x,y+1)_{4,11} = \lambda_g$$

$$\lambda(x,y+1)_{6,3} = \lambda_g,\ \lambda(x,y+1)_{6,6} = \lambda_t,\ \lambda(x,y+1)_{6,11} = \lambda_g$$

$$\lambda(x,y+1)_{8,3} = \lambda_g,\ \lambda(x,y+1)_{8,6} = \lambda_g,\ \lambda(x,y+1)_{8,11} = \lambda_t$$

The matrix $G(x,y,s|1)$ is a 1 × 12 matrix and given as

$$G(x,y,s|1) = [G(x,y,s^{eh}|1)\ \ G(x,y,s^{ef}|1)\ \ G(x,y,s^{eg}|1)\ \ G(x,y,s^{fh}|1)\ \ G(x,y,s^{gh}|1)\ \ G(x,y,s^{fg}|1)\ \ G(x,y,s^{gf}|1)\ \ G(x,y,s^{fe}|1)\ \ G(x,y,s^{ge}|1)\ \ G(x,y,s^{hf}|1)\ \ G(x,y,s^{hg}|1)\ \ G(x,y,s^{he}|1)]$$

Similarly, eq 6 can also be written as a matrix form as

$$G(x,y,s|r) = G(x,y,s)\sum_{x',y'} X\lambda(x',y')\ XG(x',y',(s+1)|r) \tag{A2}$$

The 12 × 12 matrix X rearranges the segment orientation to obtain the segment weighting factor counting from the other end of a chain, and its nonzero elements are given as

$$X_{1,12} = X_{2,8} = X_{3,9} = X_{4,10} = X_{5,11} = X_{6,7} = X_{7,6} = X_{8,2} = X_{9,3} = X_{10,4} = X_{11,5} = X_{12,1} = 1$$

Then the statistical weight of segment s ending at (x, y) is calculated with

$$G(x,y,s) = G(x,y,s|1)\ G^{-1}(x,y,s)\ WG(x,y,s|r) \tag{A3}$$

where W is a 12 × 12 matrix of $W_{i,i} = 1/12$ and all other elements are zero.

The equation for calculating volume fraction is then given by

$$\varphi(x,y,s) = C_i G(x,y,s) \tag{A4}$$

References and Notes

(1) Smith, B. L.; Schaffer, T. E.; Viani, M.; Thompson, J. B.; Frederick, N. A.; Kindt, J.; Belcher, A.; Stucky, G. D.; Morse, D. E.; Hansma, P. K. *Nature* **1999**, *399*, 761.
(2) Bates, F. S.; Fredrickson, G. H. *Annu. Rev. Phys. Chem.* **1990**, *41*, 525.
(3) Helfand, E. *J. Chem. Phys.* **1975**, *62*, 999.
(4) Hong, K. M.; Noolandi, J. *Macromolecules* **1981**, *14*, 727.
(5) Mayes, A. M.; de la Cruz, M. O. *J. Chem. Phys.* **1991**, *95*, 4670.
(6) Matsen, M. W.; Schick, M. *Phys. Rev. Lett.* **1994**, *72*, 2660.
(7) Semenov, A. N.; Vasilenko, S. V. *Sov. Phys. JETP* **1986**, *63*, 70.
(8) Williams, D. R. M.; Fredrickson, G. H. *Macromolecules* **1992**, *25*, 3561.
(9) Muller, M.; Schick, M. *Macromolecules* **1996**, *29*, 8900.
(10) Matsen, M. W. *J. Chem. Phys.* **1996**, *104*, 7758.
(11) Netz, R. R.; Schick, M. *Phys. Rev. Lett.* **1996**, *77*, 302.
(12) Matsen, M. W.; Barrett, C. *J. Chem. Phys.* **1998**, *109*, 4108.
(13) Chen, J. T.; Thomas, E. L.; Ober, C. K.; Hwang, S. S. *Macromolecules* **1995**, *28*, 1688.
(14) Chen, J. T.; Thomas, E. L.; Ober, C. K.; Mao, G. P. *Science* **1996**, *273*, 343.
(15) Radzilowski, L. H.; Stupp, S. I. *Macromolecules* **1994**, *27*, 7747.
(16) Stupp, S. I.; LeBonheur, V.; Walker, K.; Li, L. S.; Huggins, K. E.; Keser, M.; Amstutz, A. *Science* **1997**, *276*, 384.
(17) Jenekhe, S. A.; Chen, X. L. *Science* **1998**, *279*, 1903.
(18) Leermakers, F. A. M.; Scheutjens, J. M. H. M. *J. Chem. Phys.* **1989**, *89*, 3264.
(19) Evers, O. A.; Scheutjens, J. M. H. M.; Fleer, G. J. *Macromolecules* **1990**, *23*, 5221.
(20) Drolet, F.; Fredrickson, G. H. *Phys. Rev. Lett.* **1999**, *83*, 4317.
(21) Semenov, A. N. *Macromolecules* **1993**, *26*, 6617.
(22) Leibler, L. *Macromolecules* **1980**, *13*, 1602.
(23) Gido, S. P.; Thomas, E. L. *Macromolecules* **1994**, *27*, 6137.
(24) Huber, K.; Burchard, W.; Bantle, S. *Polymer* **1987**, *28*, 863.

MA010194I